Supplementary Information (SI) for ChemComm.
This journal is © The Royal Society of Chemistry 2025

Supplementary Information

Expanding Icosahedral Frameworks: Structure and Bonding of Bicapped Icosahedral Cluster [(Cp*Co)$_4$Fe(CO)B$_9$H$_{11}$]

Soumen Giri, Subhash Bairagi, Sampad Shyamal, and Sundargopal Ghosh*

Department of Chemistry, Indian Institute of Technology Madras, Chennai 600036, India, E-mail: sghosh@iitm.ac.in

Table of contents

I Experimental Details

General Procedures and Instrumentation. All manipulations were carried out under an oxygen-free Ar or N_2 atmosphere using standard Schlenk line techniques or in a glove box. Toluene, hexane, and THF were distilled from purple solutions of Na-benzophenone ketyl, while dichloromethane and $CDCl_3$ were distilled from calcium hydride under an inert atmosphere, before use. The metal precursor $[(Cp^*CoCl)_2]$[1] was synthesized by following the literature procedure. Commercially available reagents, $LiBH_4$ (2.0 M in THF) and $[Fe_3CO_{12}]$, were purchased from Sigma-Aldrich and used as received. Thin-layer chromatography (TLC) was performed on 250-μm aluminum-backed silica gel plates (Merck TLC plates) for the separation of reaction mixtures. NMR spectra were recorded on a Bruker Avance III 500 MHz spectrometer. Residual solvent peaks were used as internal references: $CDCl_3$ at δ = 7.26 ppm for ^{1}H NMR and δ = 77.1 ppm for $^{13}C\{^1H\}$ NMR. The ^{11}B decoupled ^{1}H spectrum was obtained with inverse gated decoupling (zgig) and power gated decoupling (zgpr) pulse sequences, respectively. $^{11}B\{^1H\}$ NMR spectra were processed with a backward linear prediction algorithm to eliminate the broad ^{11}B background signal of the NMR tube.[2] All pulse sequences are available in a commercial Bruker spectrometer. Electrospray ionization mass spectrometry (ESI-MS) data were collected using a XEVO G3 QTof mass spectrometer. Note that both compounds showed the desired isotopic distributions in their ESI-MS spectra. However, the additional peaks or apparent fragmentations are attributed to common background ions typically observed under ESI^+ conditions. Additionally, for compound **1**, the mass spectrum generally corresponds to the loss or addition of CO ligands, which is common in metal complexes containing coordinated CO. Furthermore, this may also be due to the high sensitivity of the samples under the detection conditions.[3] Infrared (IR) spectra were recorded using a JASCO FT/IR-4100 Fourier Transform Infrared Spectrometer. UV-vis spectra were recorded in dichloromethane using a JASCO V-650 UV-Vis Spectrophotometer. Note that no uncommon hazards are noted during the reaction.

Synthesis of 1 and **2.** In a flame-dried Schlenk tube, $[Cp^*CoCl]_2$ (0.200 g, 0.44 mmol) was suspended in 10 mL of dry toluene and charged dropwise with a lithium borohydride solution (2.0 M in THF, 0.8 mL, 1.6 mmol) at -78 °C under constant stirring. The initially brown color reaction mixture gradually turned dark brown after 1 hour. To this in situ-generated, unstable dark brown intermediate, $[Fe_3(CO)_{12}]$ (0.50 mg, 0.1 mmol) was added, and the mixture was stirred at 90 °C for 18 hours. Upon the addition of $[Fe_3(CO)_{12}]$, the color of the reaction mixture changed from dark brown to greenish brown, and after 18 hours, it turned dark green. On completion of the reaction, the solvent was removed under reduced pressure using a vacuum pump. The resulting residue was extracted using a hexane/dichloromethane mixture (90:10 v/v) through a frit containing a 3 cm bed of Celite. The filtrate was concentrated, and the residue was subjected to chromatographic purification on 250-μm aluminum-backed silica gel TLC plates. Elution with a hexane/dichloromethane (90:10 v/v) mixture afforded orange complex **1** (0.033 g, 32%), dark brown complex **2** (0.016 g, 17%), along with a few air- and moisture-sensitive products in low yields that could not be isolated. The yields of both products were calculated with respect to the starting material $[Cp^*CoCl]_2$.

Note that compound **2** does not contain Fe or CO. Therefore, we have explored the reaction of $[Cp^*CoCl]_2$ with $[LiBH_4]$ in the absence of $[Fe_3(CO)_{12}]$ under various conditions. These reactions consistently yielded the known cobaltaboranes $[(Cp^*Co)_2B_2H_6]$, *closo*-1,2,3,6-$[(Cp^*Co)_4B_2H_4]$, *closo*-2,3,4-$[(Cp^*Co)_3B_2H_4]$, and *closo*-1,2,3-$[(Cp^*Co)_3B_3H_5]$, along with some unstable species that were difficult to isolate due to their higher sensitivity and low yields.[4] However, none of these reactions led to the formation of compound **2**. As metallaborane formation reactions are typically uncontrolled and mechanistically not well understood, it remains challenging to rationalize the formation of compound **2** only when $[Cp^*CoCl]_2$ and $[LiBH_4]$ are reacted in the presence of $[Fe_3(CO)_{12}]$.

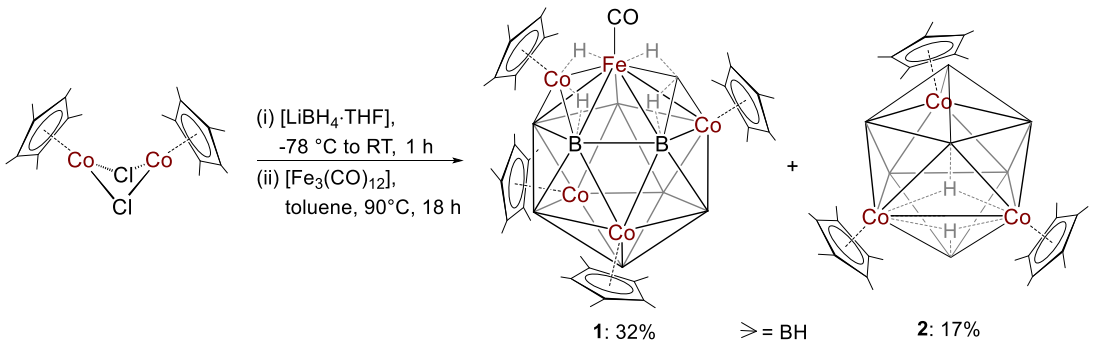

Scheme S1. Synthesis of **1** and **2**.

1: MS (ESI$^+$): *m/z* calculated for $[C_{41}H_{71}B_9OCo_4Fe + H]^+$: 970.3158, found: 970.2803; $^{11}B\{^1H\}$ NMR (160 MHz, $CDCl_3$, 22 °C): δ = 69.6 (br, 2B), 38.1 (br, 1B), 36.8 (br, 1B), 34.5 (br, 1B), 32.3 (br, 1B), 23.3 (br, 1B), and 17.3 (br, 2B) ppm; ^{11}B NMR (160 MHz, $CDCl_3$, 22 °C): δ = 70.1 (br, 2B), 37.8 (m, 2B), 34.5 (d, 1B), 32.2 (d, 1B), 23.4 (br, 1B), and 17.3 (br, 2B) ppm; ^1H NMR (500 MHz, $CDCl_3$, 22 °C): δ = 6.03 (br, B-H*t*), 3.84 (br, B-H*t*), 2.91 (br, B-H*t*), 1.87 (s,15H, Cp*), 1.72 (s, 15H, Cp*), 1.63 (s, 30H, Cp*), -0.34 (br, B-*H*-B), -9.84 (br, M-*H*-M), -12.27 (br, M-*H*-B), -12.88 (br, M-*H*-B) ppm; $^1H\{^{11}B\}$ NMR (500 MHz, $CDCl_3$, 22 °C): δ = 6.01 (br, B-H*t*), 3.96 (br, B-H*t*), 3.65 (br, B-H*t*), 3.11 (br, B-H*t*), 1.86 (s,15H, Cp*), 1.71 (s, 15H, Cp*), 1.63 (s, 30H, Cp*), -0.36 (br, B-*H*-B), -9.85 (br, M-*H*-M), -12.29 (br, M-*H*-B), -12.90 (br, M-*H*-B) ppm; $^{13}C\{^1H\}$ NMR (125 MHz, $CDCl_3$, 22 °C): δ = 97.3, 95.3, 95,1, 88.4 (s, 4 C_5Me_5), 12.4, 11.4, 10.1, 10.0 (s, 4 C_5Me_5) ppm; IR (dichloromethane, cm^{-1}): $\bar{\upsilon}$ = 2957, 2919, 2852, 2486 (B-H*t*), 2419 (B-H*t*), 2012 (terminal CO), 1948, 1461, 1376, 1259, 1090, 1023; UV-Vis (CH_2Cl_2): λ = 229, 307, 388, 459 nm.

2: MS (ESI$^+$): *m/z* calculated for $[C_{30}H_{54}B_7Co_3 - H]^+$: 666.2850, found: 666.2809; $^{11}B\{^1H\}$ NMR (160 MHz, $CDCl_3$, 22 °C): δ = 57.8 (br, 1B; B7 atom), 48.2 (br, 1B; B1 atom), 24.0 (br, 3B; B3, B5 and B6 atoms), and 9.8 (br, 2B; B2 and B4 atoms) ppm; $^{11}B\{^1H\}$ NMR (160 MHz, $CDCl_3$, 22 °C): δ = 57.8 (br, 1B), 48.2 (br, 1B), 24.0 (d, 3B), and 9.8 (br, 2B) ppm; ^1H NMR (500 MHz, $CDCl_3$, 22 °C): δ = 5.70 (br, B-H*t*), 4.69 (br, B-H*t*), 1.69 (s, 15H, Cp*), 1.62 (s, 30H, Cp*), -18.91 (s, M-*H*-B) ppm; $^{13}C\{^1H\}$ NMR (125 MHz, $CDCl_3$, 22 °C): δ = 95.6 (s, 2C_5Me_5), 93.7 (s, 1C_5Me_5), 10.5 (s, 2C_5Me_5), 9.6 (s, 1C_5Me_5) ppm; IR (dichloromethane, cm^{-1}): $\bar{\upsilon}$ = 2955, 2919, 2850, 2482 (B-H*t*), 2464 (B-H*t*), 2392 (B-H*t*), 1738, 1463, 1374, 1259, 1092, 1023; UV-Vis (CH_2Cl_2): λ = 228, 255, 290, 335, 387 nm.

I.1 UV-visible Studies

In order to investigate the optical properties of these coloured metallaborane clusters **1** and **2**, we have carried out UV-vis study in CH_2Cl_2 solution. The UV-vis absorption spectra of all the complexes were measured in the range of 200-800 nm in CH_2Cl_2 solution at 298 K (Figures S21). All of them display the most intense peaks at higher energy regions 228-307 nm due to the π–π* transition of Cp* ligands, characteristic bands for most Cp* based metal complexes.[5] The absorptions with λ>330 nm exhibit mainly two to three absorption bands. These comparatively low energy bands, around 335-483 nm, have been assigned to the charge transfer bands.[6,7] To reproduce the UV-vis spectrum and get some idea about the electronic transitions, Time-Dependent DFT formalism was used (Figures S28-S31, Tables S4-S5). The studies show that the absorption in the range of 335-483 nm may be assigned to the electronic transitions that correspond to electron density flow from the metal centers to the boron moieties.

I.2 Supplementary Data

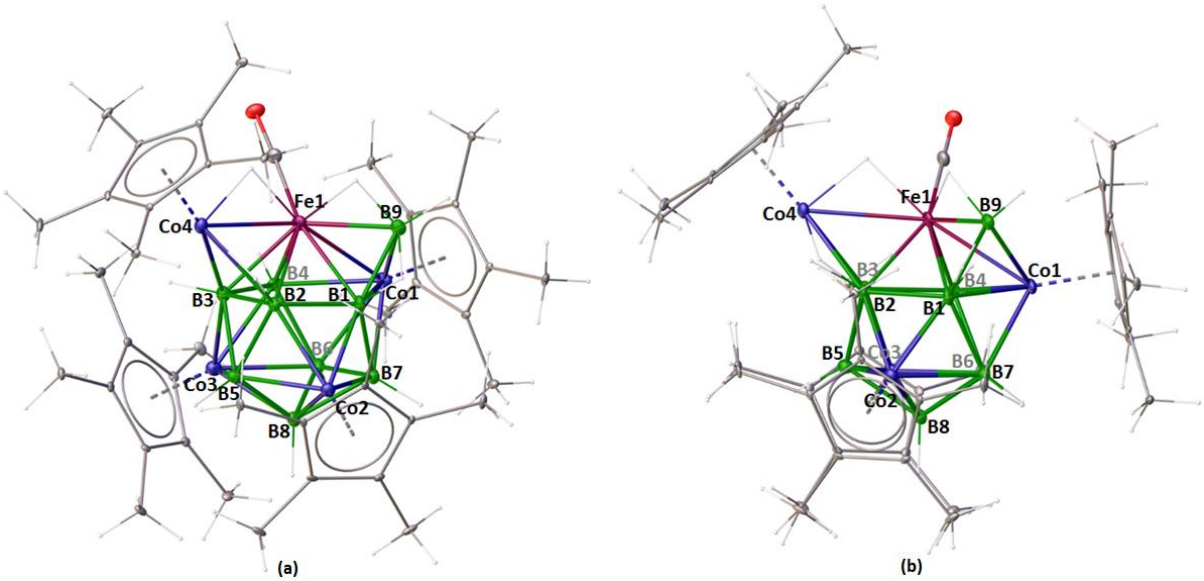

Figure S1. Molecular structure and atom labelling diagram of **1**. (a) front view (b) side view. Selected bond lengths (Å) and angles (°): Fe1−Co4 2.493(2), Fe1−B9 2.047(15), Co4−B2 2.125(12), B1−B9 1.71(2), B1−B2 1.805(17); Fe1−Co4−B2 53.03(3), Fe1−B9−B1 67.2(7).

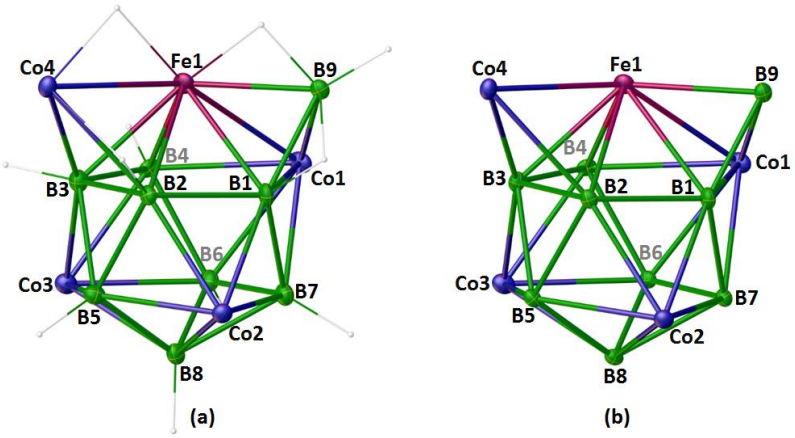

Figure S2. (a) Bicapped icosahedral core [Co_4FeB_9] of cluster **1** with hydrogens and (b) without hydrogens.

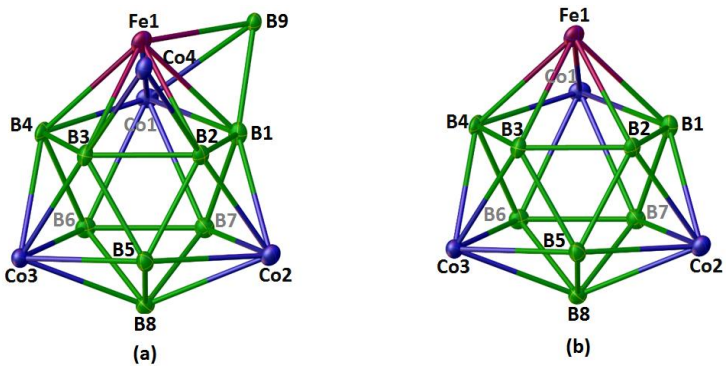

Figure S3. (a) Bicapped icosahedral core [Co_4FeB_9] and (b) icosahedral core [Co_3FeB_8] of cluster **1**, viewed perpendicular to the Co2−Co3 vector.

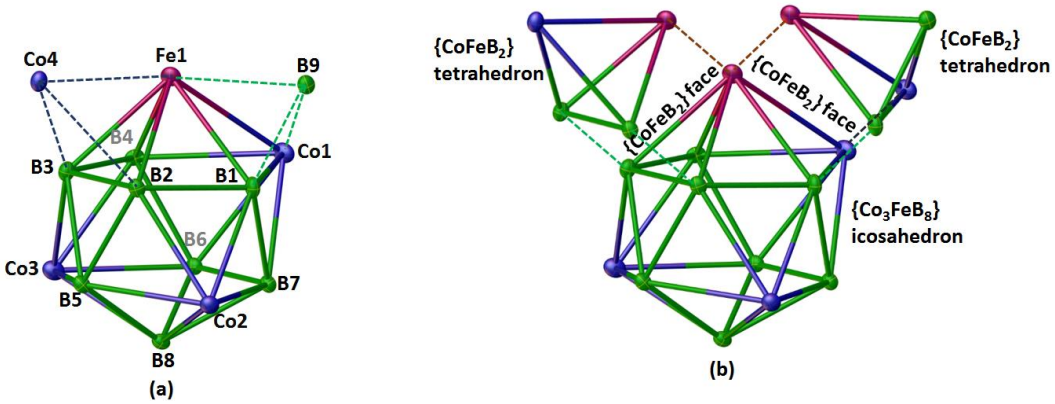

Figure S4. (a) Capping of the Co4 and B9 atoms in the icosahedral core [Co_3FeB_8] of cluster **1**. (b) Fusion of a *closo*-{Co_3FeB_8} core with two *nido*-{$CoFeB_2$} units in cluster **1**.

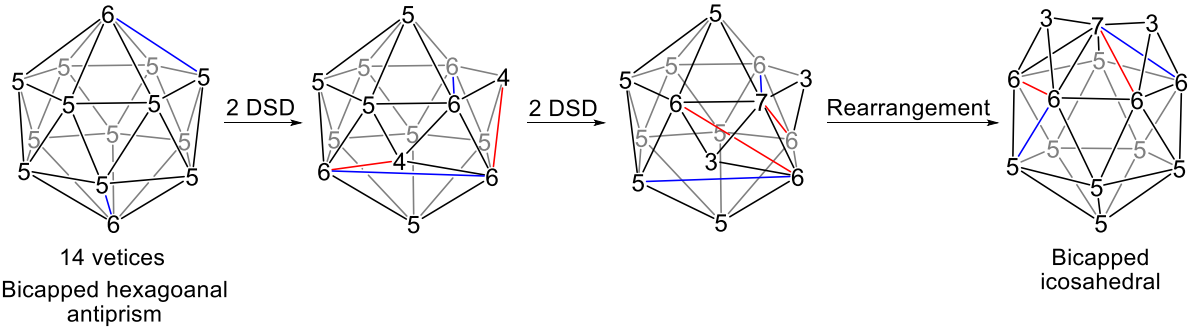

Scheme 2. Schematic representation of the formation of bicapped icosahedral cluster **1** via four diamond-square-diamond (DSD) rearrangements of the *closo*-14-vertex bicapped hexagonal antiprism.

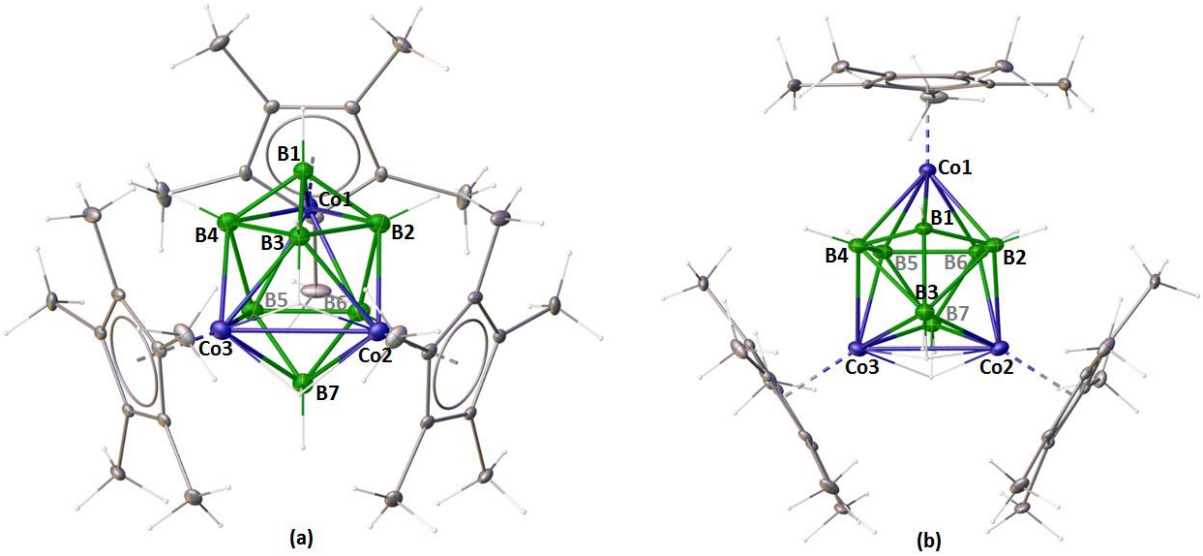

Figure S5. Molecular structure and atom labelling diagram of **2**. (a) front view (b) side view. Selected bond lengths (Å) and angles (°): Co2–Co3 2.697(17), Co3–B7 2.066(8), Co3–B4 2.122(7), B5–B6 1.816(14), B1–B3 1.597(13), Co2–Co3–B5 78.110(19).

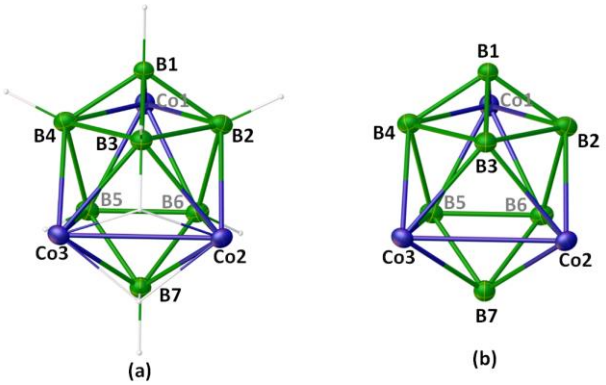

Figure S6. (a) Bicapped square antiprism core [Co_3B_7] of cluster **2** with hydrogens and (b) without hydrogens.

I.3 Spectroscopic Details

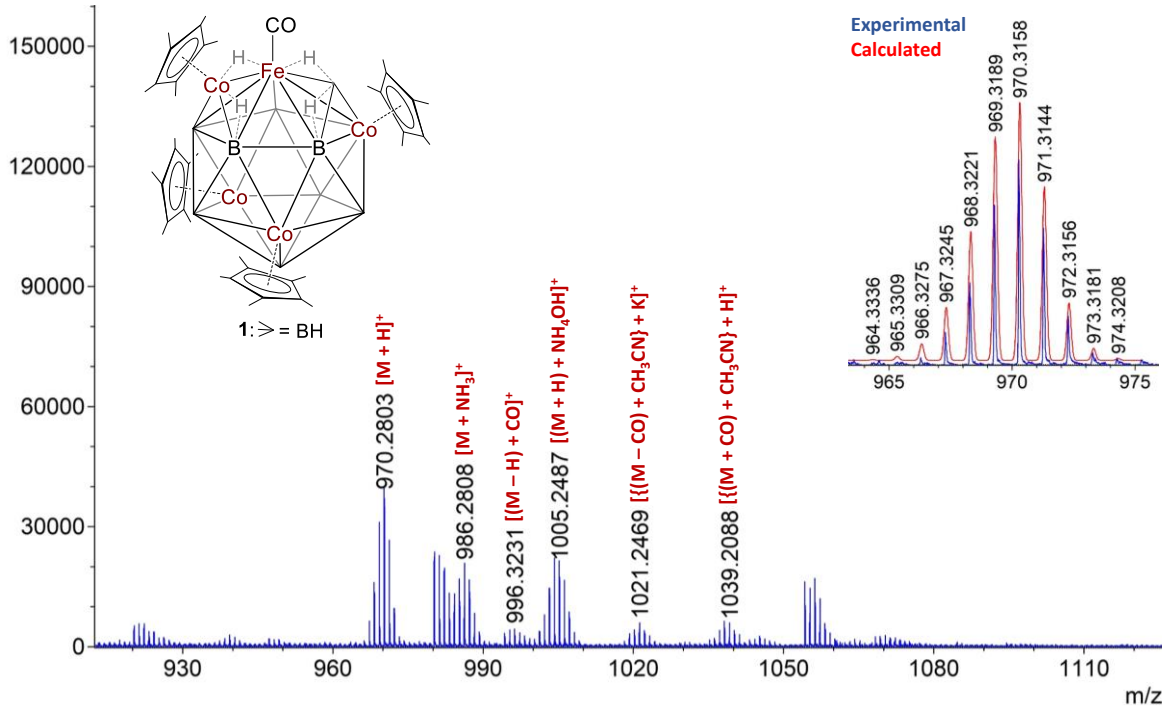

Figure S7. ESI-MS spectrum of **1**.

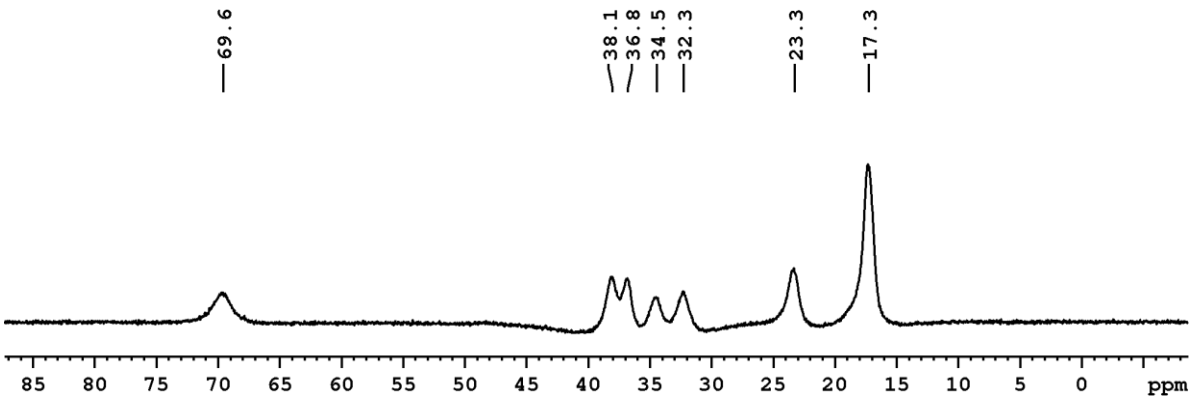

Figure S8. $^{11}B\{^1H\}$ NMR spectrum of **1** in $CDCl_3$.[2]

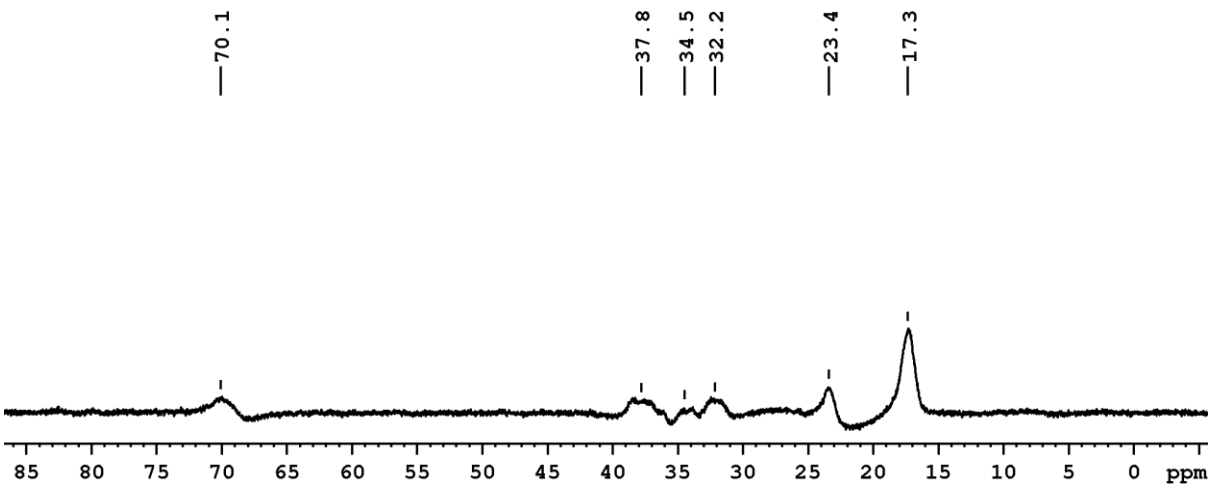

Figure S9. ^{11}B NMR spectrum of **1** in $CDCl_3$.[2]

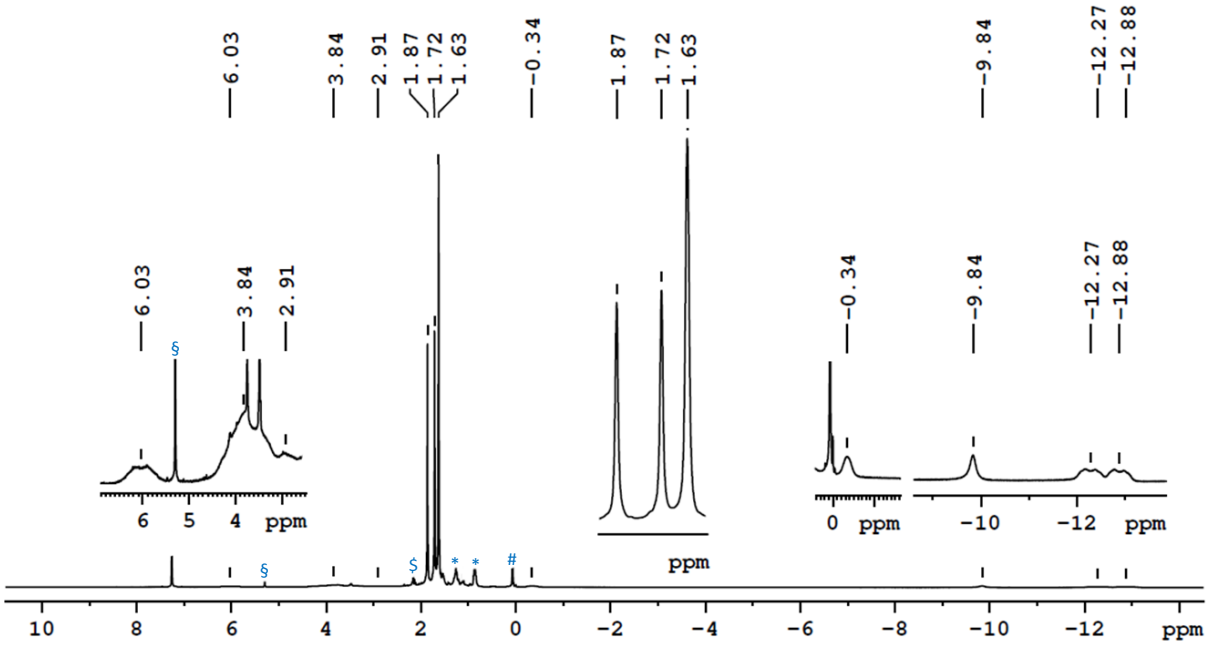

Figure S10. ^{1}H NMR spectrum of **1** in $CDCl_3$ (§CH_2Cl_2, $Acetone, *Grease, #Silicon grease).

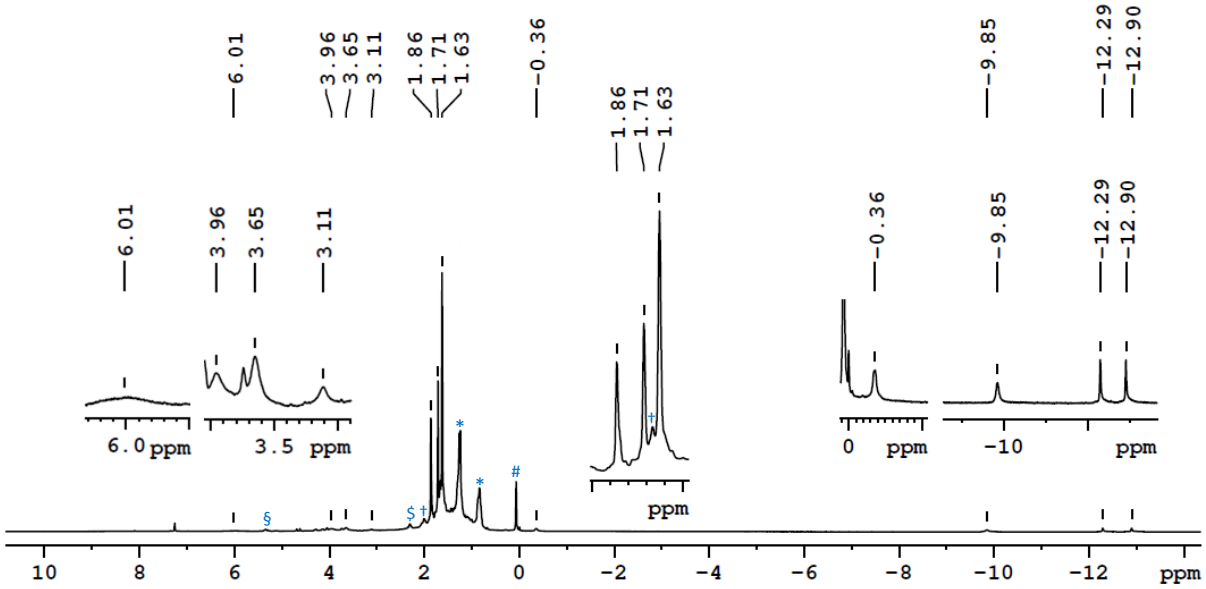

Figure S11. $^{1}H\{^{11}B\}$ NMR spectrum of **1** in $CDCl_3$ (§CH_2Cl_2, $Acetone, †Inseparable impurity, *Grease, #Silicon grease).

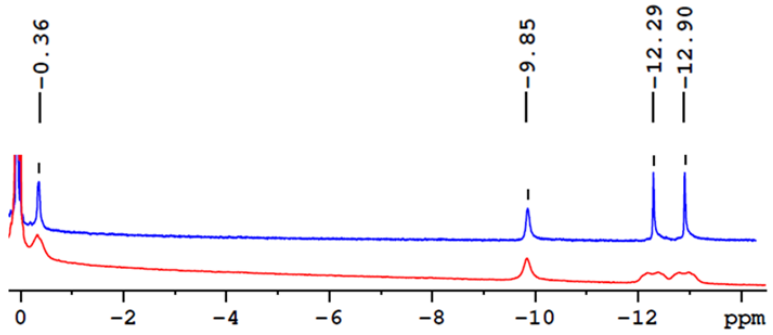

Figure S12. Stacked ^{1}H (bottom) and $^{1}H\{^{11}B\}$ NMR (top) spectra of **1** in $CDCl_3$.

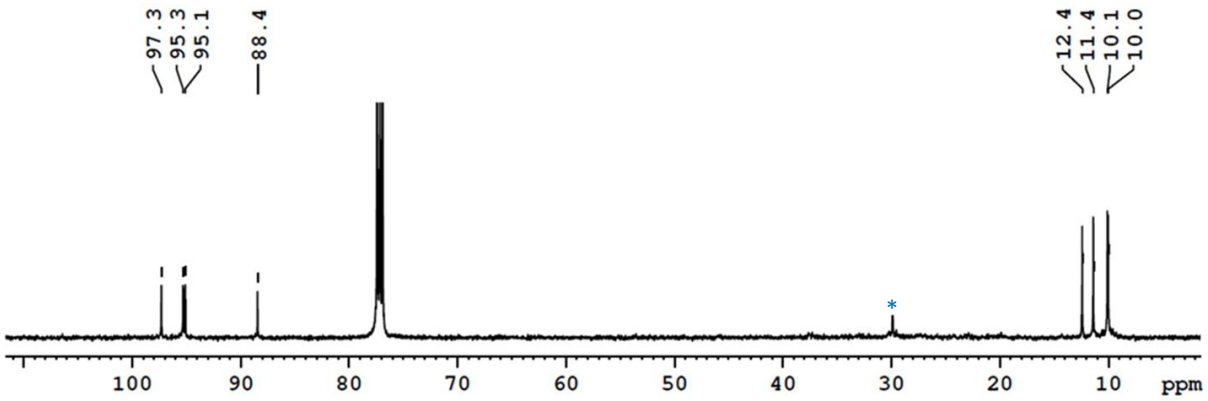

Figure S13. $^{13}C\{^{1}H\}$ NMR spectrum of **1** in $CDCl_3$ (*Grease).

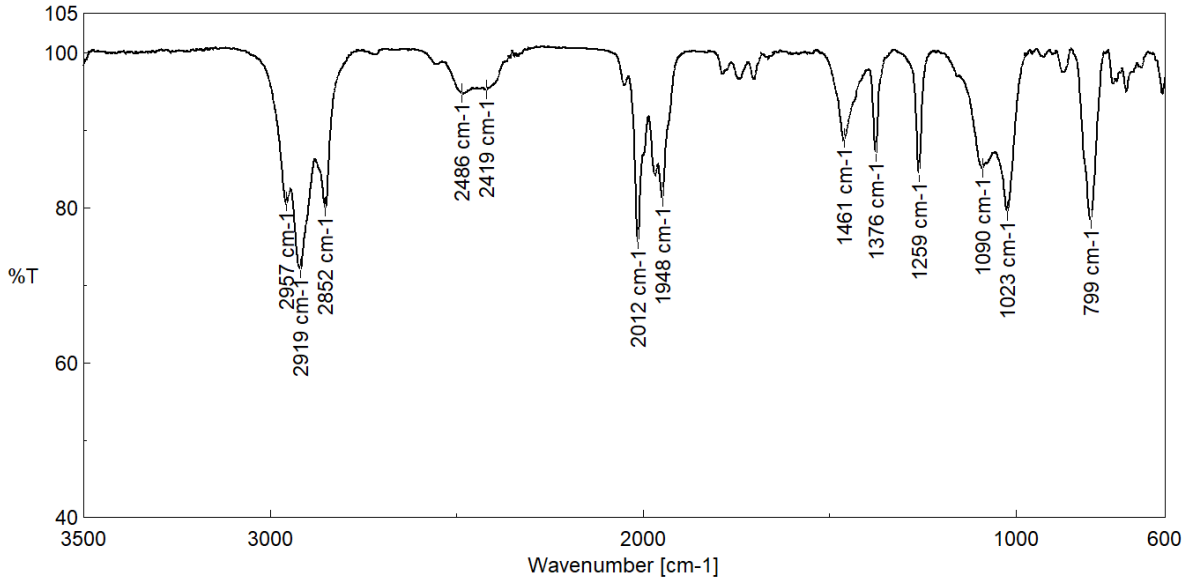

Figure S14. IR spectrum of **1**.

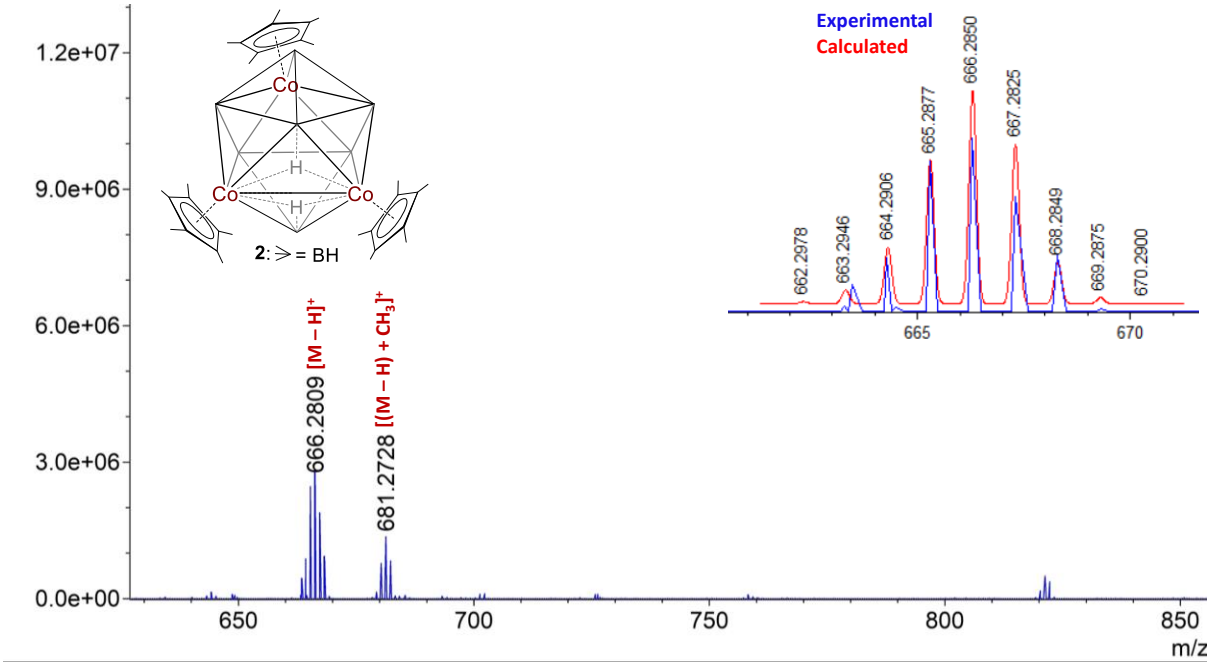

Figure S15. ESI-MS spectrum of **2**.

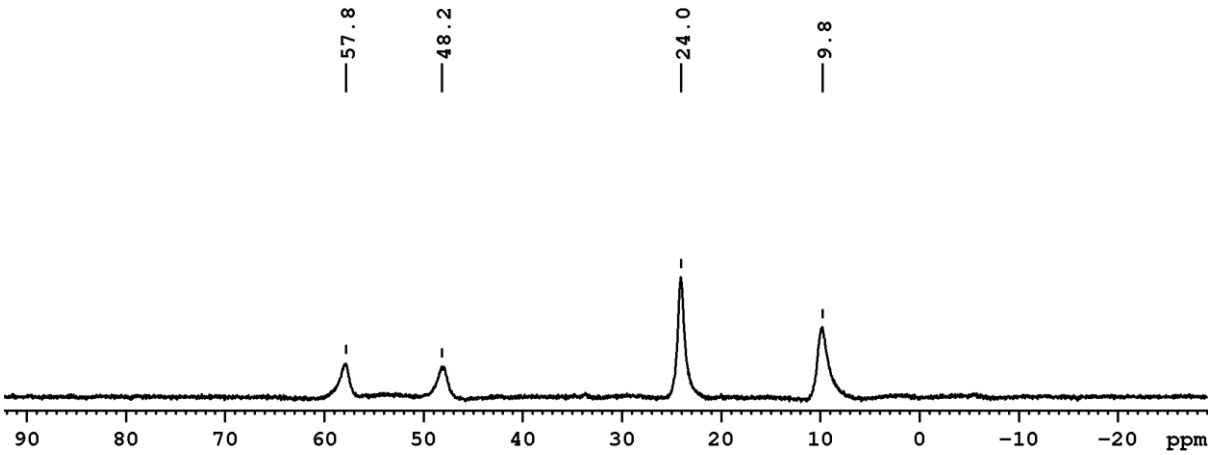

Figure S16. $^{11}B\{^{1}H\}$ NMR spectrum of **2** in $CDCl_3$.[2] The solid-state X-ray structural analysis of **2** shows that the $\{Co_3B_7\}$ core is highly symmetrical with the presence of one symmetry plane, passing through a plane containing B1, B3, B7, and Co1 atoms. This is confirmed by the $^{11}B\{^{1}H\}$, ^{1}H, and $^{13}C\{^{1}H\}$ NMR spectra of **2**. The ^{11}B resonances observed at δ = 57.8 and 48.2 ppm can be assigned to two boron atoms, B7 and B1, respectively. The resonance at δ = 9.8 ppm can be assigned to two boron atoms, B2 and B4. Besides, the $^{11}B\{^{1}H\}$ chemical shift at δ = 24.0 ppm can be assigned to three boron atoms, B3, B5, and B6, which may be due to the overlapping of the similar boron environments.

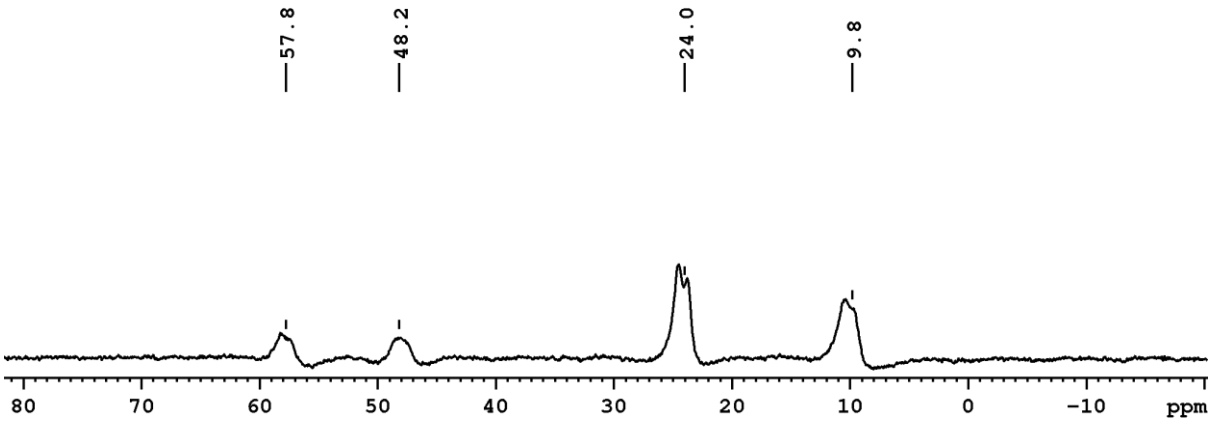

Figure S17. ^{11}B NMR spectrum of **2** in $CDCl_3$.[2]

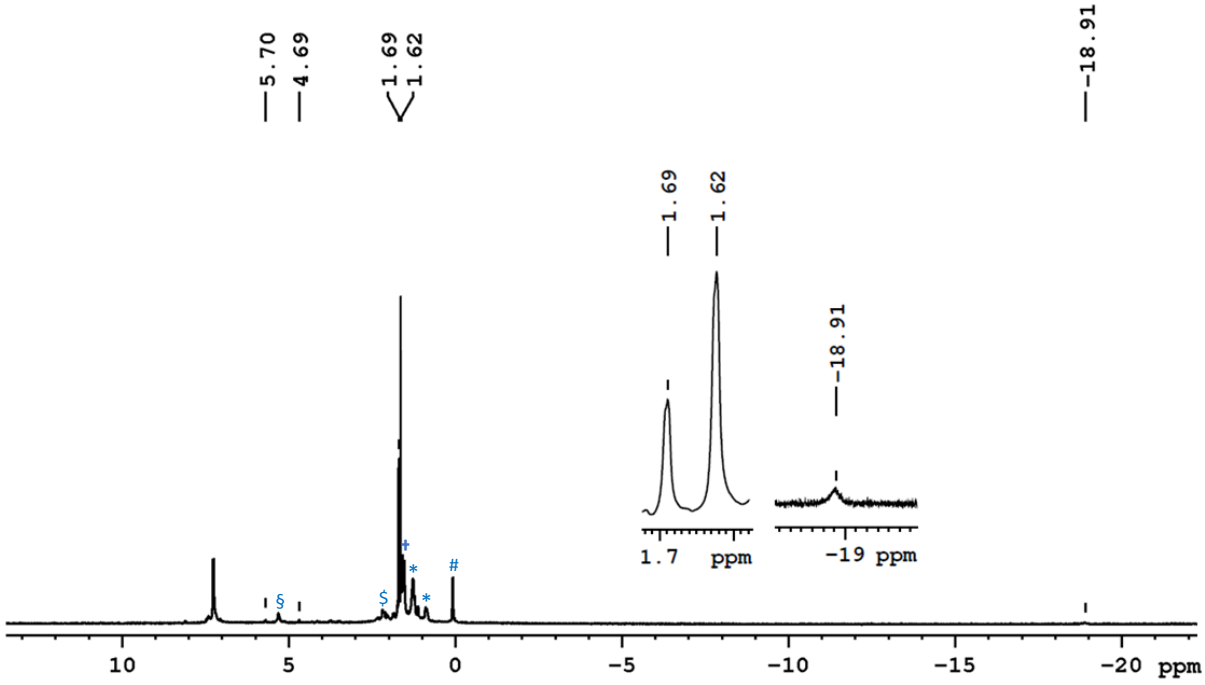

Figure S18. ^{1}H NMR spectrum of **2** in $CDCl_3$ (§CH_2Cl_2, Ş Acetone, †H_2O, *Grease, #Silicon grease).

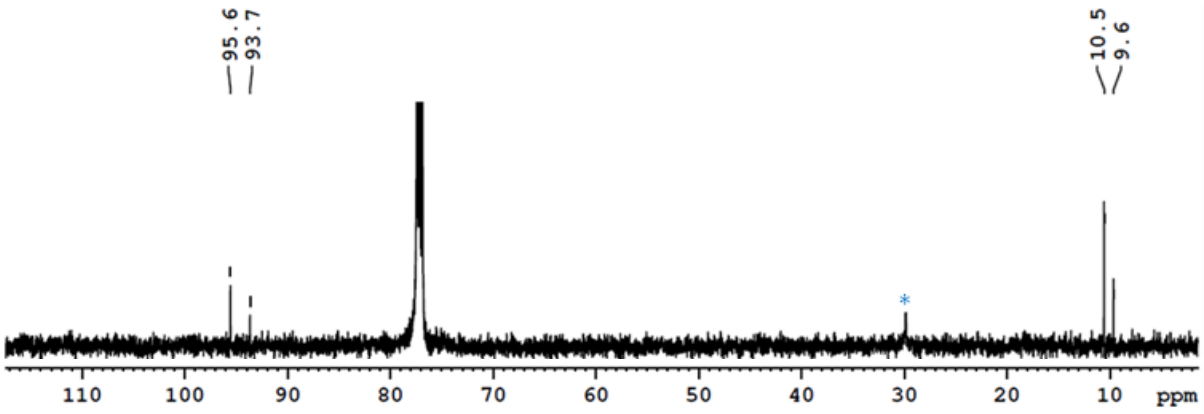

Figure S19. $^{13}C\{^{1}H\}$ NMR spectrum of **2** in $CDCl_3$ (*Grease).

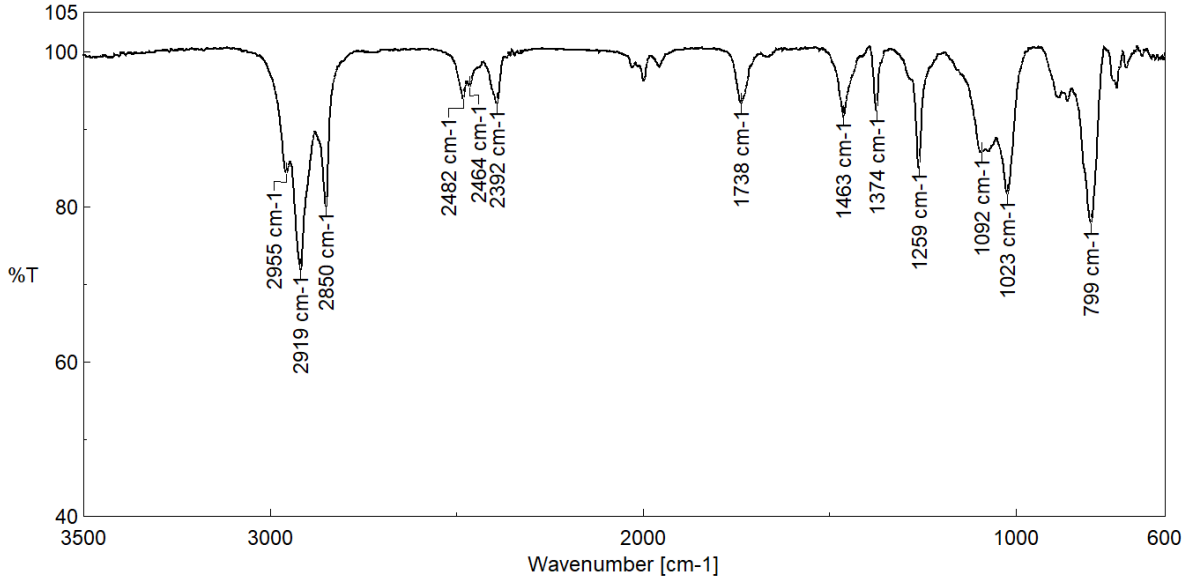

Figure S20. IR spectrum of **2**.

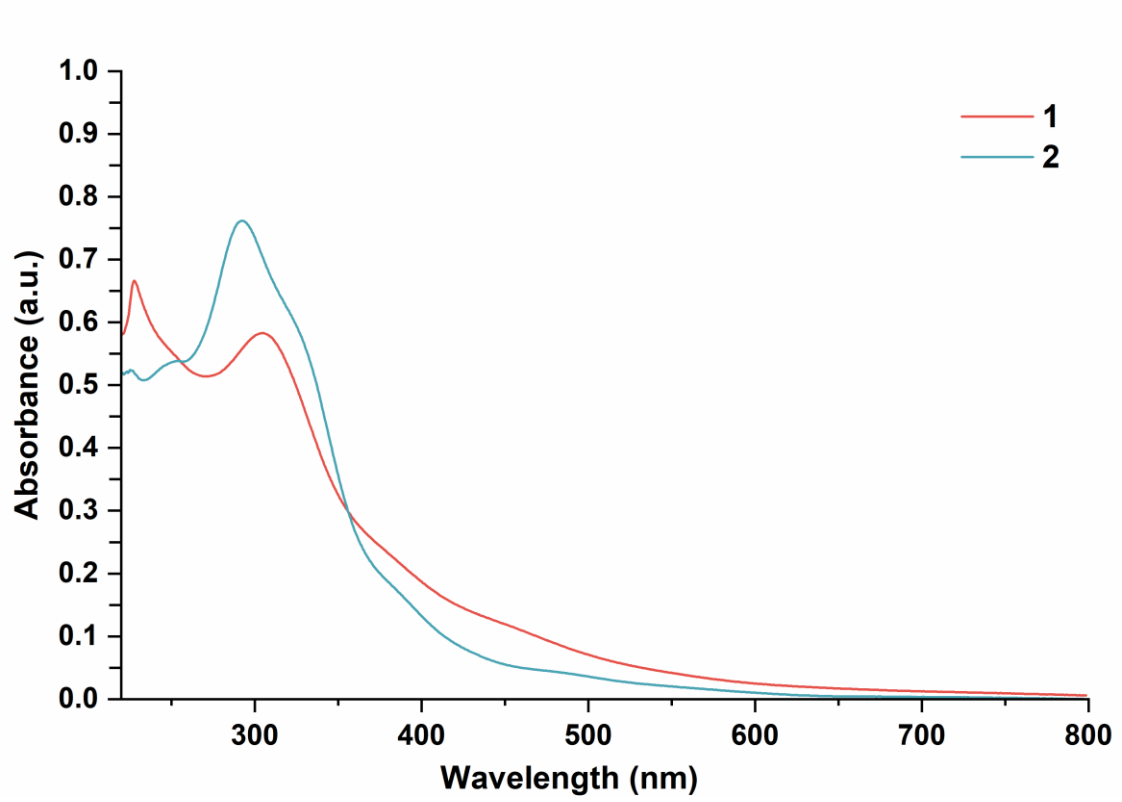

Figure S21. Combined UV-vis spectra of **1** and **2** in CH_2Cl_2.

I.4 *X-ray Analysis Details*

Suitable X-ray quality crystals of **1**, and **2** were grown by slow diffusion of a hexane-dichloromethane (80:20 v/v) solution at -5 ˚C. Crystal data of **1** was obtained and integrated using a Bruker D8 Venture, with graphite monochromated MoKα (λ = 0.71073 Å) radiation at 102(2) K. Crystal data of **2** was obtained and integrated using a Bruker Apex3 CMOS diffractometer equipped with graphite monochromated MoKα (λ = 0.71073 Å) radiation at 302(2) K. The structures were solved using SIR92[8] and refined with SHELXL-2019/2.[9] Using Olex2[10], the molecular structures were drawn. Note that compound **1** crystallizes in the triclinic system with space group P-1 with two molecules in the asymmetric unit. The crystal was twinned. Twinning has resolved, and HKLF5 format intensity data have been generated using the program PLATON. The batch scale factor (BASF) is 0.1855. The different peaks could not be modelled as solvent molecules. Hence, the squeezing of the data has been done using the program PLATON. Squeezing showed the removal of 249 electrons, equivalent to scattering by solvent molecules per unit cell. This corresponds to roughly 5 hexane molecules per unit cell. However, the removed solvents are not included in the crystallographic formula unit. One minor B-Level alert has been explained through VRF. Compound **2** crystallizes in the monoclinic system with space group P21/m with half a molecule in the asymmetric unit. Crystallographic data have been deposited with the Cambridge Crystallographic Data Center as supplementary publication no CCDC - 2464450 (**1**), and 2498867 (**2**). The data can be obtained free of charge from The Cambridge Crystallographic Data Centre via www.ccdc.cam.ac.uk/data_request/cif.

Crystal data for **1**: $C_{41}H_{71}B_9Co_4FeO$, M_r.= 968.83, triclinic, space group *P -1*, a = 15.677(2) Å, b = 17.2637(19) Å, c = 19.000(2) Å, α = 82.268(4)°, β = 78.144(4)°, γ = 89.950(4)°, V = 4984.8(11) Å^3, Z = 4, ρ_{calcd} = 1.291 g/cm^3, μ = 1.616 mm^{-1}, *F(000)* = 2016, R_1 = 0.1024, wR_2 = 0.2372, 217162 independent reflections [2θ ≤ 50.4°] and 1089 parameters.

Crystal data for **2**: $C_{30}H_{54}B_7Co_3$, M_r.= 667.19, monoclinic, space group *P 21/m*, a = 8.3355(13) Å, b = 18.415(3) Å, c = 11.3221(18) Å, α = 90°, β = 108.900(5)°, γ = 90°, V = 1644.3(4) Å^3, Z = 2, ρ_{calcd} = 1.348 g/cm^3, μ = 1.515 mm^{-1}, *F(000)* = 700, R_1 = 0.0639, wR_2 = 0.1461, 2984 independent reflections [2θ ≤ 49.8°] and 203 parameters.

II Computational Details

All molecular geometries were fully optimized using the Gaussian 09 program suite[11] with the BP86 functional[12] and the def2-SVP basis set, obtained from the EMSL Basis Set Exchange Library[13]. Geometry optimizations were carried out in the gas phase (without solvent effects), starting from the corresponding X-ray crystallographic coordinates. During the optimization of molecule **1**, the Co118···H123 distance was constrained and optimized. Vibrational frequency calculations were performed at the same level of theory to confirm that all stationary points correspond to true minima on the potential energy hypersurface (no imaginary frequencies). Natural bond orbital (NBO) analyses [14] were conducted within Gaussian 09 to obtain Wiberg bond indices (WBIs).[15] To gain deeper insight into the bonding characteristics, the topological properties of the electron density (ρ) derived from the optimized wavefunctions were analysed using the Quantum Theory of Atoms in Molecules (QTAIM).[16] QTAIM analyses were performed with the Multiwfn program (version 3.4),[17] using wavefunctions generated at the same level of theory as the geometry optimizations. All optimized structures and orbital visualizations were produced using GaussView[18] and Chemcraft.[19]

Table.S1. Selected geometrical parameters[a] and Wiberg bond indices (WBI) of **1**, **2**, **3a**, and **3b**.

1				**2**			
	Expt.	Cal.	WBI		Expt.	Cal.	WBI
Co4-Fe1	2.493	2.555	0.391	Co2-Co3	2.697	2.698	0.330
Co4-B2	2.153	2.141	0.311	Co2-B2	2.122	2.177	0.387
Co4-B3	2.183	2.277	0.238	Co2-B3	2.137	2.320	0.257
B9-Fe1	2.062	2.049	0.491	Co2-B6	2.135	2.180	0.375
B9-Co1	2.221	2.132	0.435	Co2-B7	2.066	2.126	0.398
B9-B1	2.099	1.708	0.639	B5-B6	1.816	1.831	0.499
Fe1-B1	2.099	2.115	0.405	B5-B7	1.719	1.744	0.623
Fe1-B2	2.095	2.114	0.391	B1-Co1	1.971	1.972	0.515
Fe1-C_{CO}	1.742	1.753	1.371	B1-B2	1.587	1.729	0.615
B1-B2	1.818	1.789	0.564	B1-B3	1.597	1.656	0.691
B1-Co2	1.998	2.007	0.439	B2-B3	1.937	1.902	0.507
B8-Co2	2.115	2.116	0.398				
B8-B5	1.793	1.811	0.570				

[a] Note that the B1-B9 bond becomes shorter in clusters **1** in the optimized geometries as compared to the solid-state X-ray structure.

Table S2. Selected experimental and Calculated bond angles of **1** and **2**.

1			**2**		
	Expt.	Cal.		Expt.	Cal.
Fe1-Co4-B2	52.99	52.59	Co2-Co3-B5	78.085	78.526
B2-Co4-B3	46.32	46.00	Co3-B5-B6	101.915	101.474
Fe1-B9-B1	67.04	67.83	B5-B6-Co2	101.915	101.472
Fe1-B9-Co1	69.52	67.26	Co2-B7-Co3-	81.488	78.528
B1-B9-Co1	63.018	66.35	Co2-B7-B6	67.976	67.726
Co2-B5-Co3	126.20	125.95	B2-Co1-B4	77.123	76.966
Co4-Fe1-Co1	151.17	149.51			
Fe-C_{CO}-O_{CO}	178.27	175.61			

Table S3. Calculated natural charges (q) and natural valence population (Pop) of **1** and **2**.

1			**2**		
	q	Pop(val)		q	Pop(val)
Fe1	-0.958	8.973	Co1	-0.129	9.136
Co1	0.089	8.922	Co2	-0.00004	9.003
Co2	-0.062	9.071	Co3	-0.00001	9.003
Co3	0.006	9.006	B1	-0.126	3.089
Co4	0.218	8.785	B2	-0.129	3.093
B1	-0.109	3.064	B3	-0.205	3.172
B2	-0.147	3.101	B4	-0.129	3.093
B3	-0.239	3.201	B5	-0.161	3.127
B4	-0.018	2.986	B6	-0.161	3.127
B5	-0.068	3.033	B7	-0.138	3.102
B6	-0.156	3.120			
B7	-0.124	3.089			
B8	-0.120	3.085			
B9	-0.147	3.029			
C_{CO}	0.694	6.487			
O_{CO}	-0.498	3.239			

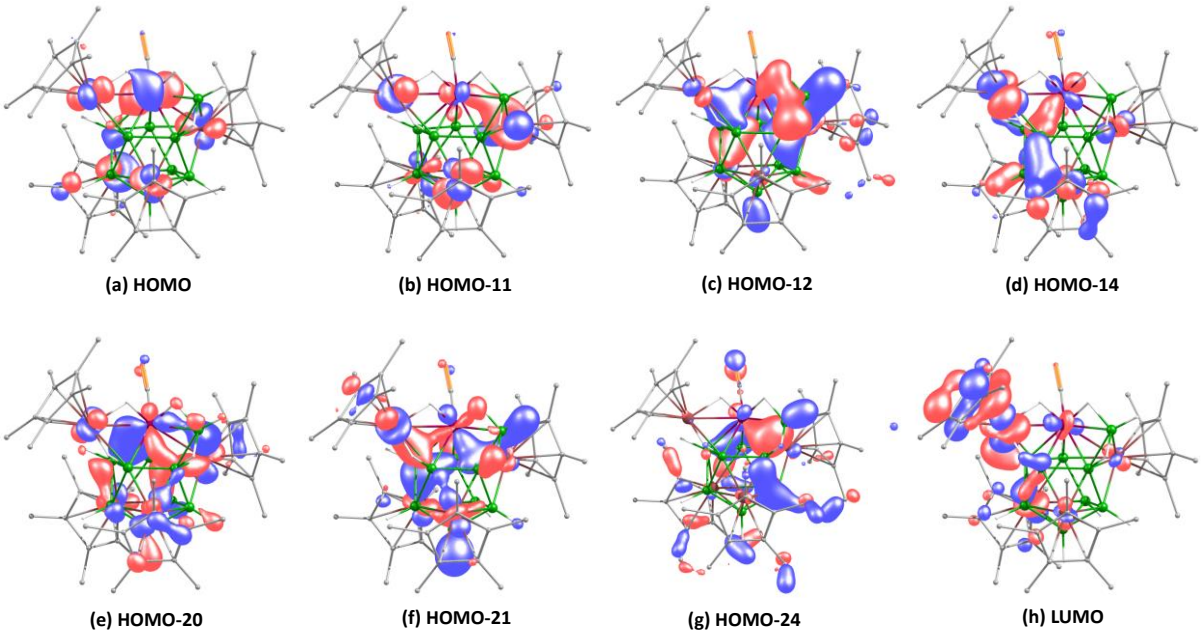

Figure S22. Selected molecular orbitals of **1** (isocontour values: ±0.045 [e.bohr^{-3}]$^{1/2}$).

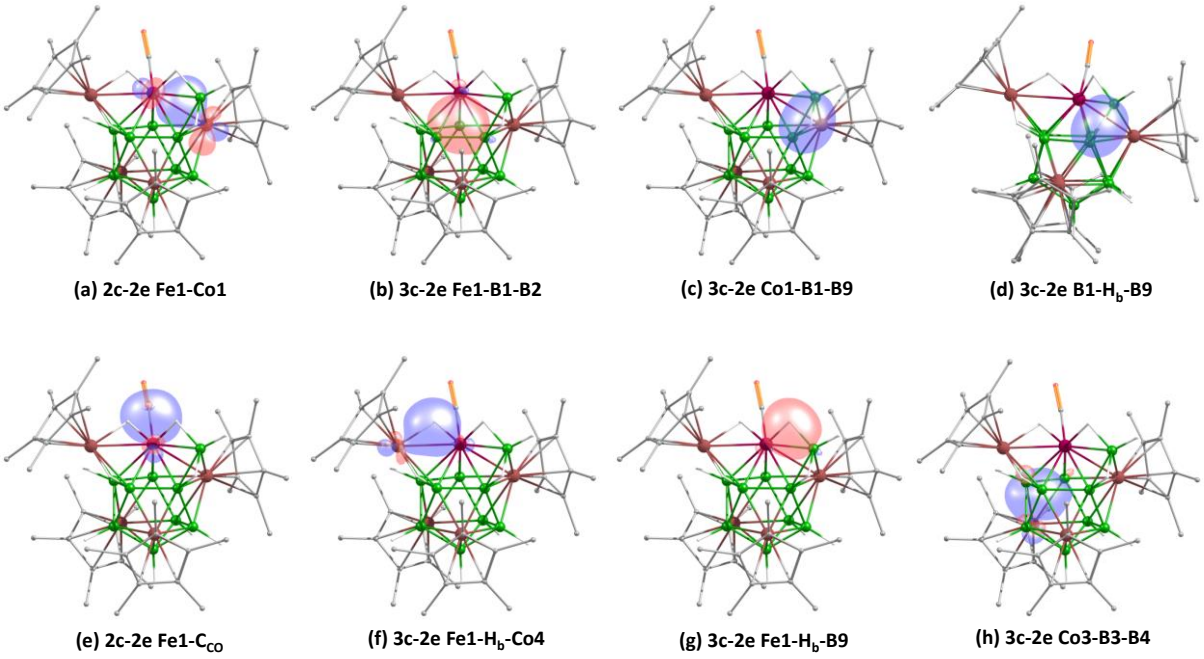

Figure S23. Selected NBO interactions of **1** (isocontour values: ±0.045 [e.bohr^{-3}]$^{1/2}$).

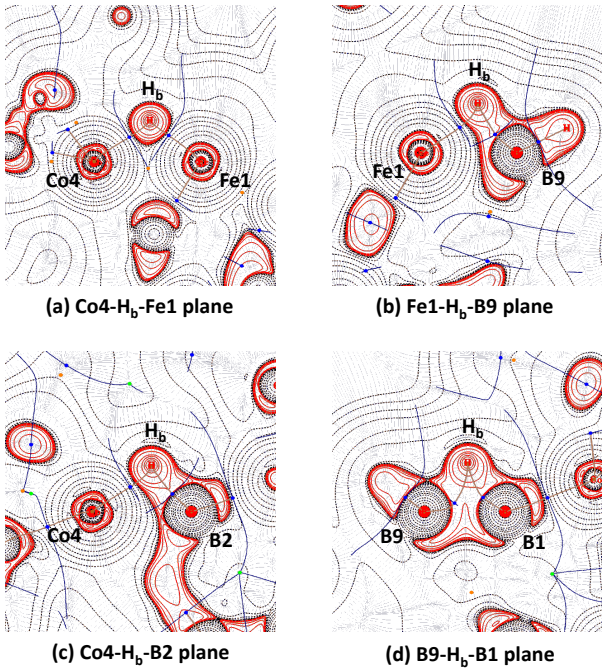

Figure S24. Contour-line diagram of the Laplacian of the electron density of **1** in selected planes. The solid brown lines are bond paths, whereas blue dots indicate the bond-critical points (BCP). Solid red lines indicate the areas of charge concentration ($\nabla^2\rho(r) < 0$), while dashed black lines show the areas of charge depletion ($\nabla^2\rho(r) > 0$).

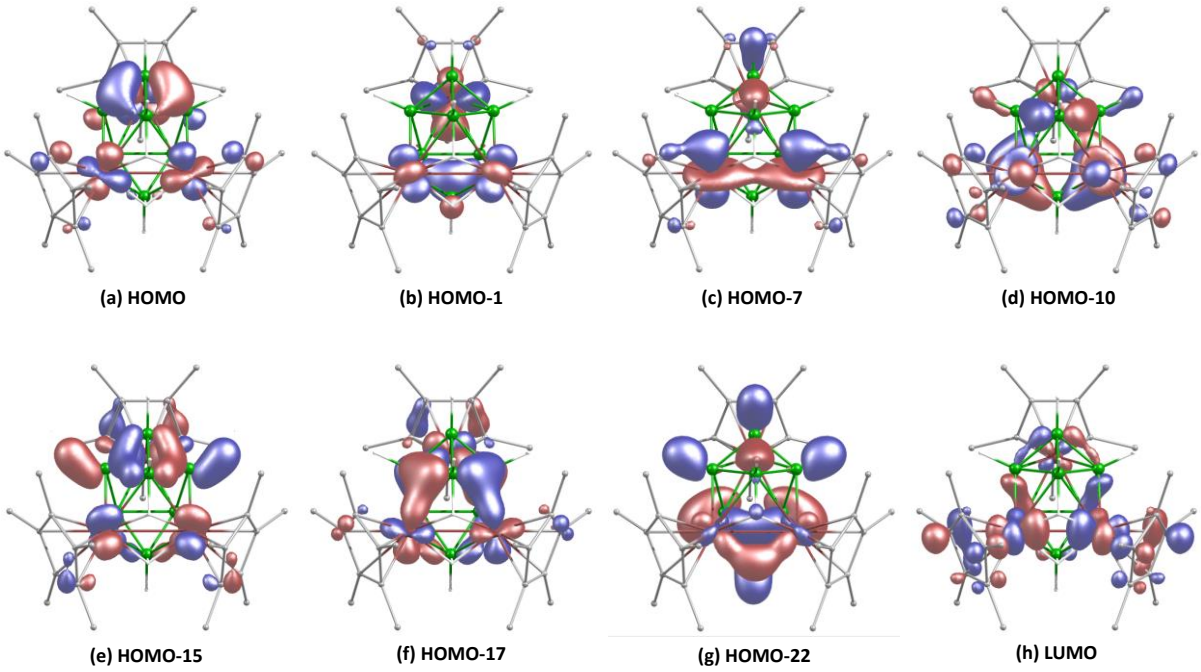

Figure S25. Selected molecular orbitals of **2** (isocontour values: ±0.045 [e.bohr^{-3}]$^{1/2}$).

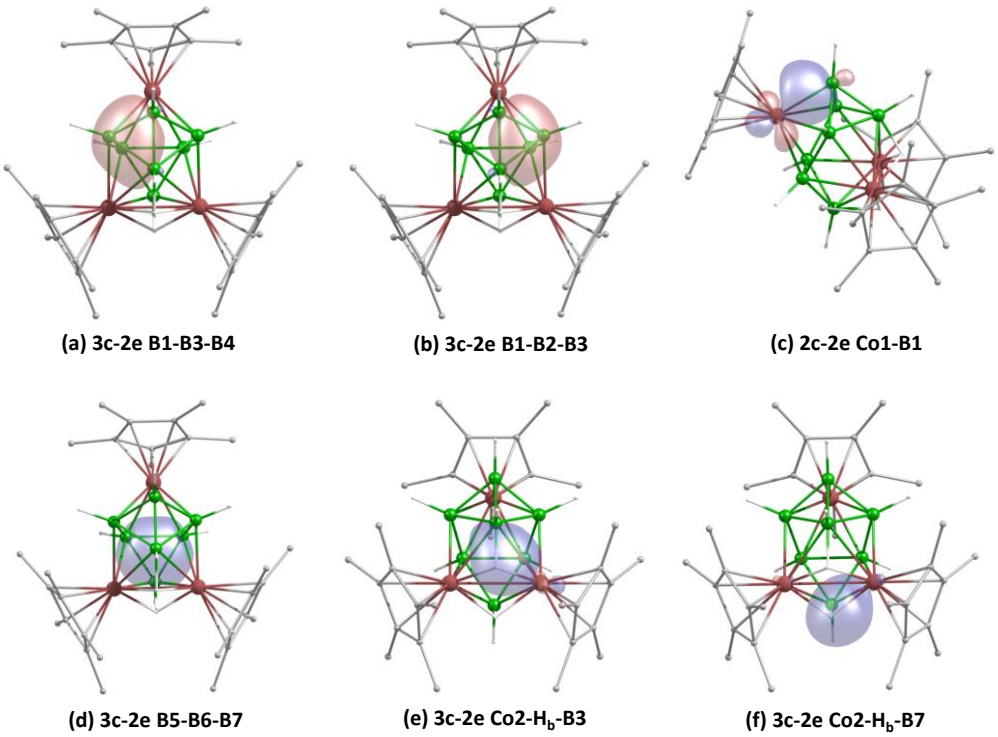

Figure S26. Selected NBO interactions of **2** (isocontour values: ±0.045 [e.bohr^{-3}]$^{1/2}$).

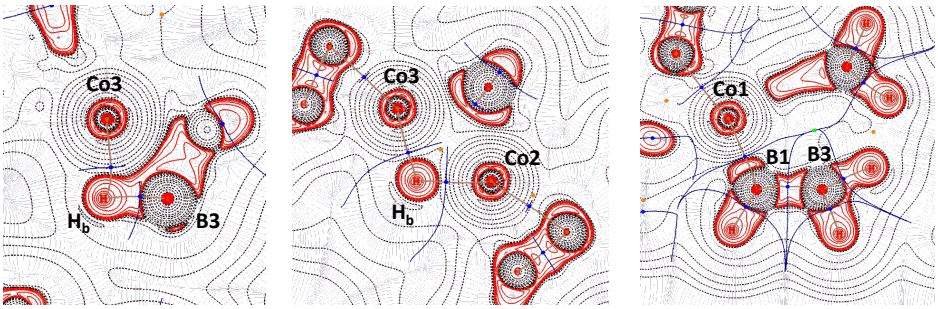

(a) Co3-H_b-B3 plane (b) Co3-H_b-Co2 plane (c) Co1-B1-B3 plane

Figure S27. Contour-line diagram of the Laplacian of the electron density of **2** in selected planes. The solid brown lines are bond paths, whereas blue dots indicate the bond-critical points (BCP). Solid red lines indicate the areas of charge concentration ($\nabla^2\rho(r) < 0$), while dashed black lines show the areas of charge depletion ($\nabla^2\rho(r) > 0$).

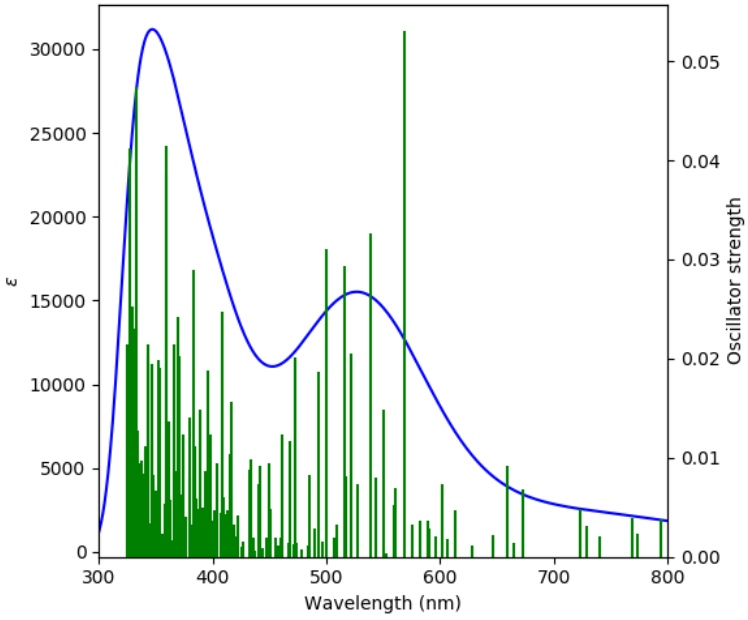

Figure S28. Absorption spectrum of **1** computed at TD-DFT-BP86/Def2-SVP level of theory (ε in $LM^{-1}cm^{-1}$).

Table S4. TD-DFT calculated energies (excitation energy (eV), λ_{calc} (nm)), oscillator strength (*f*), and main composition of the first UV−vis electronic excitations for **1**. Experimental absorption wavelengths (λ_{exp}, nm) of **1** are given for comparison.

No	Excitation Energy (eV)	Wavelength λ (nm)		Main electronic transition (% weight) [b]
		Calc. (*f*) [a]	Expt.	
1	2.182	568 (0.053)		HOMO-12→LUMO (28)
				HOMO-3→LUMO+2 (19)
2	2.298	539 (0.033)		HOMO-16→LUMO (23)
				HOMO-15→LUMO (21)
3	2.375	522 (0.020)		HOMO-16→LUMO (11)
				HOMO-11→LUMO+1 (26)
				HOMO-11→LUMO+1 (26)
				HOMO-4→LUMO+2 (13)
4	2.402	516 (0.029)		HOMO-16→LUMO (18)
				HOMO-11→LUMO+1 (24)
5	2.481	500 (0.031)		HOMO-12→LUMO+1 (65)
6	2.623	473 (0.020)	459	HOMO-18→LUMO (56)
7	3.031	409 (0.025)		HOMO-8→LUMO+4 (11)
				HOMO→LUMO+7 (19)
8	3.238	383 (0.029)	388	HOMO-26→LUMO (11)
				HOMO-20→LUMO+1 (19)
				HOMO-2→LUMO+7 (11)
9	3.453	359 (0.042)		HOMO-27→LUMO (31)
				HOMO-12→LUMO+4 (16)
10	3.456	359 (0.038)		HOMO-27→LUMO (17)
				HOMO-17→LUMO+2 (11)
				HOMO-15→LUMO+3 (24)
				HOMO-12→LUMO+4 (11)

[a]Oscillator strength greater than 0.020 and [b]Components with greater than 10% contribution shown.

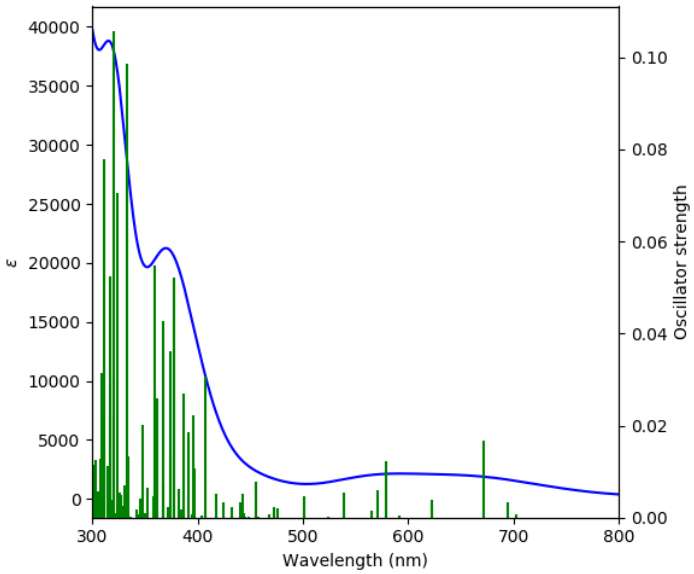

Figure S29. Absorption spectrum of **2** computed at TD-DFT-BP86/Def2-SVP level of theory (ε in $LM^{-1}cm^{-1}$).

Table S5. TD-DFT calculated energies (excitation energy (eV), λ_{calc} (nm)), oscillator strength (*f*), and main composition of the first UV−vis electronic excitations for **2**. Experimental absorption wavelengths (λ_{exp}, nm) of **2** are given for comparison.

No	Excitation Energy (eV)	Wavelength λ (nm)		Main electronic transition (% weight) [b]
		Calc. (*f*) [a]	Expt.	
1	1.844	672 (0.017)		HOMO→LUMO+1 (54)
				HOMO→LUMO+2 (36)
2	2.142	579 (0.012)		HOMO-5→LUMO (94)
				HOMO-1→LUMO+7 (19)
3	2.472	501 (0.05)		HOMO-1→LUMO+3 (90)
4	3.045	407 (0.031)		HOMO-4→LUMO+3 (35)
				HOMO-3→LUMO+3 (36)
5	3.286	377 (0.052)	387	HOMO-8→LUMO+1 (34)
				HOMO-6→LUMO+1 (11)
6	3.310	374 (0.036)		HOMO-9→LUMO+1 (39)
				HOMO-6→LUMO+3 (26)
7	3.380	367 (0.043)		HOMO-11→LUMO+1 (15)
				HOMO-9→LUMO+2 (34)
				HOMO-7→LUMO+2 (13)
8	3.454	359 (0.055)		HOMO-10→LUMO+1 (53)
				HOMO-9→LUMO+3 (17)
9	3.729	332 (0.098)	335	HOMO-12→LUMO+2 (12)
				HOMO-9→LUMO+3 (41)
10	3.873	320 (0.106)		HOMO-10→LUMO+3 (23)
				HOMO-5→LUMO+5 (12)
				HOMO-3→LUMO+4 (13)
				HOMO-1→LUMO+5 (15)

[a]Oscillator strength greater than 0.010 and [b]Components with greater than 10% contribution shown.

III Cartesian Coordinates of all Optimized Structures

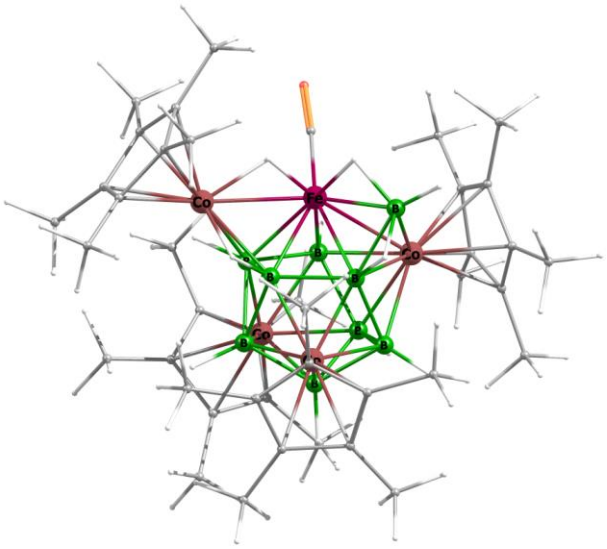

Figure S30. Optimized geometry of **1**.

Total energy = -8698.21259461 a.u.

Cartesian coordinates for the calculated structure **1** (in Å)

C	-3.890938000	-2.385264000	-0.123874000
C	-4.437034000	-1.142293000	0.405969000
C	-4.647491000	-0.240353000	-0.690692000
C	-4.237399000	-0.918754000	-1.916264000
C	-3.812161000	-2.256103000	-1.560289000
C	-4.835963000	-0.890291000	1.828895000
H	-4.684539000	0.166741000	2.120790000
H	-4.262800000	-1.521709000	2.534300000
H	-5.914131000	-1.127873000	1.974181000
C	-5.325705000	1.095013000	-0.603837000
H	-6.431530000	0.965558000	-0.608438000
H	-5.070311000	1.746864000	-1.461409000
H	-5.058437000	1.637160000	0.323942000
C	-4.368766000	-0.385484000	-3.312908000
H	-3.562632000	-0.763139000	-3.972669000
H	-4.329140000	0.721346000	-3.336191000
H	-5.339478000	-0.691289000	-3.764634000
C	-3.437259000	-3.347752000	-2.520224000
H	-4.338748000	-3.945016000	-2.783095000
H	-2.689622000	-4.039378000	-2.087273000
H	-3.018551000	-2.944674000	-3.462942000
C	-3.587344000	-3.627228000	0.661642000
H	-4.467538000	-4.308999000	0.672945000
H	-3.334473000	-3.393064000	1.713897000
H	-2.732427000	-4.185755000	0.233551000
C	1.197549000	-1.051631000	3.959581000
C	-0.234782000	-1.191216000	3.915109000
C	-0.818966000	0.128530000	4.046288000
C	0.256143000	1.079024000	4.133125000
C	1.507319000	0.353516000	4.073737000
C	2.161461000	-2.198094000	4.011416000
H	3.206393000	-1.863660000	3.868362000
H	1.935645000	-2.951219000	3.228429000
H	2.105704000	-2.713184000	4.996557000
C	-0.961521000	-2.504634000	3.870360000
H	-0.531324000	-3.179226000	3.102478000
H	-2.035475000	-2.370583000	3.632747000
H	-0.901602000	-3.030091000	4.849983000
C	-2.273013000	0.468813000	4.189056000
H	-2.490665000	0.863204000	5.206161000
H	-2.916652000	-0.417591000	4.033013000
H	-2.580661000	1.243687000	3.455546000
C	0.103900000	2.548702000	4.390996000
H	-0.822382000	2.948892000	3.934466000
H	0.956223000	3.123871000	3.980213000
H	0.055771000	2.752718000	5.484913000
C	2.865414000	0.968438000	4.238615000
H	3.035522000	1.278486000	5.294006000
H	2.978456000	1.867496000	3.599162000
H	3.671958000	0.262849000	3.961446000
C	-1.383754000	3.800962000	-0.911703000
C	-0.820765000	3.418147000	-2.187417000
C	0.600739000	3.689026000	-2.144046000
C	0.915559000	4.229249000	-0.843551000
C	-0.309647000	4.287300000	-0.079741000
C	-2.833364000	3.803296000	-0.527372000
H	-3.452418000	3.275339000	-1.277253000
H	-2.990490000	3.305284000	0.452378000
H	-3.224819000	4.841491000	-0.445088000
C	-1.589712000	2.937981000	-3.386111000
H	-2.479259000	2.346662000	-3.089950000
H	-1.945549000	3.790910000	-4.006761000
H	-0.971738000	2.290969000	-4.040702000
C	1.568422000	3.533289000	-3.281950000
H	1.710958000	4.497651000	-3.818998000
H	1.216802000	2.791660000	-4.026579000
H	2.562358000	3.199588000	-2.923068000
C	2.250920000	4.732851000	-0.380722000

H	2.470998000	4.392871000	0.651786000
H	2.279583000	5.845408000	-0.386387000
H	3.071699000	4.371662000	-1.029405000
C	-0.464787000	4.882599000	1.287996000
H	0.440321000	4.721291000	1.904897000
H	-1.323359000	4.438691000	1.828851000
H	-0.638575000	5.980559000	1.222315000
C	3.214852000	-2.096528000	-2.394081000
C	3.859447000	-0.792099000	-2.348988000
C	4.343752000	-0.589761000	-1.012505000
C	4.000027000	-1.761171000	-0.233456000
C	3.295392000	-2.681526000	-1.078893000
C	2.814746000	-2.863389000	-3.625093000
H	3.583522000	-3.637768000	-3.844141000
H	2.732258000	-2.214544000	-4.516727000
H	1.846505000	-3.386336000	-3.494472000
C	4.119170000	0.113223000	-3.518123000
H	4.116383000	1.177944000	-3.210784000
H	3.354546000	-0.006791000	-4.310360000
H	5.111811000	-0.099846000	-3.974673000
C	5.198438000	0.541047000	-0.524823000
H	6.251782000	0.204167000	-0.399299000
H	4.842256000	0.915840000	0.456446000
H	5.198966000	1.393057000	-1.230528000
C	4.517836000	-2.092086000	1.131765000
H	5.457948000	-2.682541000	1.038846000
H	3.794544000	-2.702522000	1.703429000
H	4.744910000	-1.184763000	1.722168000
C	2.921710000	-4.082459000	-0.695132000
H	2.260373000	-4.559652000	-1.441524000
H	2.391612000	-4.107301000	0.278329000
H	3.833699000	-4.713602000	-0.596243000
C	-0.227508000	-3.127974000	-0.890864000
B	1.999815000	0.138080000	0.964339000
H	3.054393000	0.067731000	1.567228000
B	0.880767000	-1.320006000	0.734673000
H	1.193647000	-2.389430000	1.248037000
B	-0.821919000	-0.586546000	0.731264000
B	-0.690641000	1.238067000	1.012301000
H	-1.616102000	1.825935000	1.567710000
B	-0.948339000	0.521797000	-0.592080000
B	1.070530000	1.648232000	1.112123000
H	1.522255000	2.578125000	1.770402000
B	0.610701000	0.530732000	-1.469001000
B	1.889489000	1.246807000	-0.422722000
H	2.836585000	1.908956000	-0.810006000
B	0.901744000	-0.653234000	-2.665609000
O	-0.334008000	-4.291226000	-0.733010000
Fe	-0.200858000	-1.388165000	-1.102779000
Co	-2.639350000	-0.790676000	-0.625156000
Co	0.388521000	0.036364000	2.278064000
Co	0.067652000	2.277512000	-0.641917000
Co	2.193000000	-0.809276000	-0.976071000
H	-0.146405000	-1.501426000	-2.714185000
H	-1.778350000	-1.161583000	1.296144000
H	-2.149454000	0.679842000	-1.127062000
H	1.322472000	-0.725782000	-3.802701000
H	0.609942000	0.702863000	-2.766899000
H	-1.650262000	-1.585994000	-1.693930000

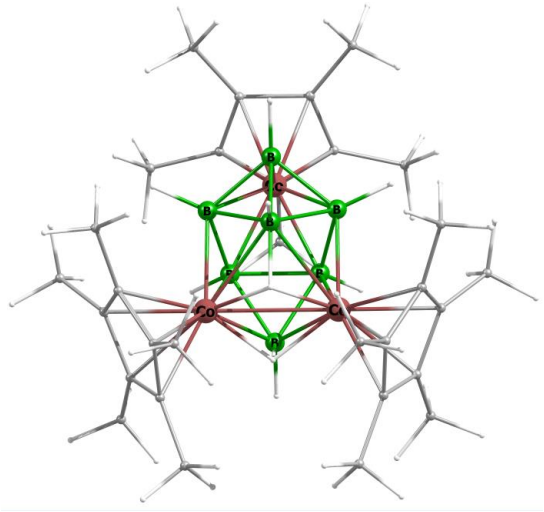

Figure S31. Optimized geometry of **2**

Total energy = -5497.44536398 a.u.

Cartesian coordinates for the calculated structure **2** (in Å)

C	1.686235000	-3.081076000	-1.131604000
C	2.888360000	-2.355012000	-0.814199000
C	3.008415000	-2.270570000	0.627081000
C	1.855717000	-2.909230000	1.209039000
C	1.041451000	-3.424358000	0.122825000
C	1.246548000	-3.501463000	-2.502512000
H	1.655175000	-2.830858000	-3.283318000
H	0.142901000	-3.477295000	-2.592536000
H	1.590882000	-4.535195000	-2.730010000
C	3.898241000	-1.885843000	-1.822117000
H	4.599582000	-1.144680000	-1.392715000
H	3.412650000	-1.422065000	-2.704184000

H	4.507639000	-2.739919000	-2.192558000
C	4.194455000	-1.770430000	1.398653000
H	3.896564000	-1.241146000	2.325152000
H	4.823904000	-1.084768000	0.800485000
H	4.840480000	-2.624313000	1.702767000
C	1.597792000	-3.150457000	2.667204000
H	1.890671000	-4.185414000	2.954472000
H	0.522906000	-3.025055000	2.906345000
H	2.165213000	-2.448261000	3.307936000
C	-0.127322000	-4.343486000	0.313261000
H	0.232834000	-5.327094000	0.690353000
H	-0.675946000	-4.517057000	-0.630288000
H	-0.844378000	-3.938259000	1.053824000
C	-4.139586000	0.724536000	-0.811079000
C	-3.926094000	1.166702000	0.549813000
C	-3.800328000	-0.001335000	1.391553000
C	-4.405150000	1.619182000	-1.987668000
H	-4.152054000	1.121068000	-2.943639000
H	-3.803748000	2.548701000	-1.933604000
H	-5.477737000	1.913978000	-2.032242000
C	-3.934463000	2.594538000	1.012590000
H	-3.525448000	3.274354000	0.238899000
H	-3.329567000	2.729330000	1.930942000
H	-4.970443000	2.932869000	1.240843000
C	-3.641062000	-0.002869000	2.884932000
B	0.579129000	-0.000168000	1.533014000
H	0.955660000	-0.000351000	2.693802000
B	-1.369581000	0.000368000	-1.854016000
H	-1.882254000	0.000568000	-2.955736000
B	0.296296000	0.000136000	-1.671188000
H	0.864567000	0.000236000	-2.760584000
B	-0.821397000	1.315858000	-0.873364000
H	-1.150937000	2.425782000	-1.257229000
B	-0.764410000	0.915437000	0.901377000
H	-1.122676000	1.712833000	1.764773000
Co	1.172592000	-1.349106000	-0.000039000
Co	-2.289960000	0.000152000	-0.110220000
H	1.752906000	-0.000050000	0.850409000
H	1.497369000	0.000020000	-0.991818000
C	-4.139784000	-0.722032000	-0.812735000
C	-3.926314000	-1.167401000	0.547124000
C	-4.405800000	-1.613985000	-1.991268000
H	-4.153973000	-1.113379000	-2.946260000
H	-3.803715000	-2.543226000	-1.940025000
H	-5.478232000	-1.909396000	-2.035534000
C	-3.934834000	-2.596396000	1.006327000
H	-3.524658000	-3.274123000	0.231411000
H	-3.331011000	-2.733318000	1.925073000
H	-4.970980000	-2.935624000	1.232469000
H	-3.081052000	0.887330000	3.233848000
H	-3.084167000	-0.895577000	3.232384000
H	-4.629481000	-0.001575000	3.397406000
B	-0.821515000	-1.315477000	-0.873716000
H	-1.151111000	-2.425263000	-1.257957000
B	-0.764534000	-0.915487000	0.901171000
H	-1.122908000	-1.713112000	1.764302000
C	1.685231000	3.081772000	-1.130931000
C	2.887628000	2.355347000	-0.815573000
C	3.009508000	2.269864000	0.625491000
C	1.857633000	2.908281000	1.209392000
C	1.042002000	3.424181000	0.124572000
C	1.244290000	3.503393000	-2.501046000
H	1.650224000	2.832039000	-3.282620000
H	0.140482000	3.481675000	-2.589420000
H	1.590606000	4.536403000	-2.728834000
C	3.896030000	1.886665000	-1.825195000
H	4.597991000	1.145276000	-1.397221000
H	3.409079000	1.423327000	-2.706753000
H	4.504860000	2.740923000	-2.196148000
C	4.196654000	1.769136000	1.394962000
H	3.900215000	1.240555000	2.322312000
H	4.824349000	1.082668000	0.795853000
H	4.844007000	2.622637000	1.697331000
C	1.601516000	3.148465000	2.668059000
H	1.895067000	4.183100000	2.955800000
H	0.526879000	3.023218000	2.908396000
H	2.169473000	2.445592000	3.307577000
C	-0.126686000	4.342985000	0.317073000
H	0.233693000	5.326407000	0.694429000
H	-0.676478000	4.517082000	-0.625699000
H	-0.842772000	3.937052000	1.058196000
Co	1.172748000	1.349080000	0.000207000

References

1 U. Kölle, F. Khouzami, B. Fuss, *Angew. Chem. Int. Ed.* 1982, **21**, 131–132.

2 (*a*) J. J. Led and H. Gesmar, *Chem. Rev.*, 1991, **91**, 1413–1426; (*b*) L. Yang, R. Simionescu, A. Lough and H. Yan, *Dyes Pigm.*, 2011, **91**, 264–267; (*c*) R. Weiss and R. N. Grimes, *J. Am. Chem. Soc.*, 1978, **100**, 1401–1405.

3 a) R. Prakash, A. N. Pradhan, M. Jash, S. Kahlal, M. Cordier, T. Roisnel, J.-F. Halet, and S. Ghosh, *Inorg. Chem.*, 2020, **59**, 3, 1917–1927; b) S. Bairagi, S. Giri, D. K. Patel, D. Luong, B. P. T. Fokwa and S. Ghosh, *Dalton Trans.*, 2024, **53**, 3191–3205.

4 a) Y. Nishihara, K. J. Deck, M. Shang, T. P. Fehlner, B. S. Haggerty and A. L. Rheingold, *Organometallics*, 1994, **13**, 4510–4552; b) T. P. Fehlner, *Organometallics*, 2000, **19**, 2643−2651.

5 P. Govindaswamy, Y. A. Mozharivskyj, M. R. Kollipara, *Polyhedron* 2005, **24**, 1710.

6 a) C. E. Rao, S. K. Barik, K. Yuvaraj, K. Bakthavachalam, T. Roisnel, V. Dorcet, J.-F. Halet, Ghosh, *Eur. J. Inorg. Chem.* **2016**, 4913; b) A. Haridas, S. Kar, B. Raghavendra, T. Roisnel, V. Dorcet, S. Ghosh, *Organometallics* 2020, **39**, 58.

7 a) S. Bairagi, A. N. Pradhan, M. Cordier, T. Roisnel and S. Ghosh, *Eur. J. Inorg. Chem.,* 2023, **26**, e202300060; b) S. Bairagi, D. K. Patel, D. Chatterjee, M. Kučeráková, J. Macháček, T. Base, T. Pradeep and S. Ghosh, *Chem. Sci.*, 2025, **16**, 14127–14139; c) S. Bairagi, S. Giri, G. Joshi, E. D. Jemmis and S. Ghosh, *Angew. Chem. Int. Ed.*, 2024, e202417170; d) S. Bairagi, D. Chatterjee, S. Giri and S. Ghosh, *Chem. Commun.*, 2025, **61**, 3696–3699.

8 A. Altomare, G. Cascarano, C. Giacovazzo, A. Guagliardi, M. C. Burla, G. Polidori and M. Camalli, *J. Appl. Crystallogr*., 1994, **27**, 435.

9 G. M. Sheldrick, *Acta Cryst.*, 2015, **C71**, 3.

10 O. V. Dolomanov, L. J. Bourhis, R. J. Gildea, J. A. K. Howard and H. Puschmann, *J. Appl. Cryst*., 2009, **42**, 339.

11 M. J. Frisch, G. W. Trucks, H. B. Schlegel, G. E. Scuseria, M. A. Robb, J. R. Cheeseman, G. Scalmani, V. Barone, B. Mennucci, G. A. Petersson, H. Nakatsuji, M. Caricato, X. Li, H. P. Hratchian, A. F. Izmaylov, J. Bloino, G. Zheng, J. L. Sonnenberg, M. Hada, M. Ehara, K. Toyota, R. Fukuda, J. Hasegawa, M. Ishida, T. Nakajima, Y. Honda, O. Kitao, H. Nakai, T. Vreven, J. A. Montgomery Jr., J. E. Peralta, F. Ogliaro, M. Bearpark, J. J. Heyd, E. Brothers, K. N. Kudin, V. N. Staroverov, R. Kobayashi, J. Normand, K. Raghavachari, A. Rendell, J. C. Burant, S. S. Iyengar, J. Tomasi, M. Cossi, N. Rega, J. M. Millam, M. Klene, J. E. Knox, J. B. Cross, V. Bakken, C. Adamo, J. Jaramillo, R. Gomperts, R. E. Stratmann, O. Yazyev, A. J. Austin, R. Cammi, C. Pomelli, J. W. Ochterski, R. L. Martin, K. Morokuma, V. G. Zakrzewski, G. A. Voth, P. Salvador, J. J. Dannenberg, S. Dapprich, A. D. Daniels, Ö. Farkas, J. B. Foresman, J. V. Ortiz, J. Cioslowski, D. J. Fox, *Gaussian 09, Revision C.01*, Gaussian, Inc., Wallingford, CT, 2010.

12 (a) H. L. Schmider, A. D. Becke, *J. Chem. Phys.* 1998, **108**, 9624; (b) J. P. Perdew, *Phys. Rev. B: Condens. Matter Mater. Phys.* 1986, **33**, 8822.

13 EMSL Basis Set Exchange Library. https://bse.pnl.gov/bse/portal

14 (*a*) E. D. Glendening, A. E. Reed, J. E. Carpenter and F. Weinhold, *NBO Program 3.1*, W. T. Madison, 1988; (*b*) A. E. Reed, F. Weinhold and L. A. Curtiss, *Chem. Rev.*, 1988, **88**, 899; (*c*) F. Weinhold and R. Landis, *Valency and bonding: A natural bond orbital donor-acceptor perspective;* Cambridge University Press: Cambridge, U.K, 2005.

15 K. Wiberg, *Tetrahedron*, 1968, **24**, 1083.

16 (*a*) R. F. W. Bader, *Atoms in Molecules: A Quantum Theory*; Oxford University Press: Oxford, U. K., 1990; (*b*) R. F. W. Bader, *J. Phys. Chem. A.*, 1998, **102**, 7314; (*c*) R. F. W. Bader, *Chem. Rev.*, 1991, **91**, 893.

17 T. Lu, F. Chen, *J. Comput. Chem.*, 2012, ***33***, 580.

18 I. I. Dennington, R. T. Keith, J. Millam, K. Eppinnett, W. L. Hovell and R. Gilliland, *GaussView, Version 3.09*; Semichem Inc.: Shawnee Mission, KS, 2003.

19 G. A. Zhurko, http://www.chemcraftprog.com.